The EMBO Journal (2007) 26, 3686–3698 | © 2007 European Molecular Biology Organization | All Rights Reserved 0261-4189/07
www.embojournal.org

THE EMBO JOURNAL

Deregulation of tumor angiogenesis and blockade of tumor growth in PPARβ-deficient mice

Sabine Müller-Brüsselbach[1,6], Martin Kömhoff[2,6], Markus Rieck[1,6], Wolfgang Meissner[1], Kerstin Kaddatz[1], Jürgen Adamkiewicz[1], Boris Keil[3], Klaus J Klose[3], Roland Moll[4], Andrew D Burdick[5], Jeffrey M Peters[5] and Rolf Müller[1,*]

[1]Institute of Molecular Biology and Tumor Research (IMT), Philipps-University, Marburg, Germany, [2]Department of Pediatrics, Philipps-University, Baldingerstrasse, Marburg, Germany, [3]Department of Diagnostic Radiology, Small Animal and Molecular Imaging Center, Philipps-University, Baldingerstrasse, Marburg, Germany, [4]Institute of Pathology, Philipps-University, Baldingerstrasse, Marburg, Germany and [5]Department of Veterinary and Biomedical Sciences and Center for Molecular Toxicology and Carcinogenesis, The Pennsylvania State University, University Park, PA, USA

The peroxisome proliferator-activated receptor-β (PPARβ) has been implicated in tumorigenesis, but its precise role remains unclear. Here, we show that the growth of syngeneic *Pparb* wild-type tumors is impaired in *Pparb*$^{-/-}$ mice, concomitant with a diminished blood flow and an abundance of hyperplastic microvascular structures. Matrigel plugs containing pro-angiogenic growth factors harbor increased numbers of morphologically immature, proliferating endothelial cells in *Pparb*$^{-/-}$ mice, and retroviral transduction of *Pparb* triggers microvessel maturation. We have identified the *Cdkn1c* gene encoding the cell cycle inhibitor p57^{Kip2} as a PPARβ target gene and a mediator of the PPARβ-mediated inhibition of cell proliferation, which provides a possible mechanistic explanation for the observed tumor endothelial hyperplasia and deregulation of tumor angiogenesis in *Pparb*$^{-/-}$ mice. Our data point to an unexpected essential role for PPARβ in constraining tumor endothelial cell proliferation to allow for the formation of functional tumor microvessels.

The EMBO Journal (2007) **26,** 3686–3698. doi:10.1038/sj.emboj.7601803; Published online 19 July 2007
Subject Categories: molecular biology of disease
Keywords: hyperplasia; peroxisome proliferator-activated receptor β/δ; p57^{KIP2}/*Cdkn1c*; tumor angiogenesis; tumor growth

Introduction

Peroxisome proliferator-activated receptors (PPARs) are nuclear receptors that function as transcription factors and modulate target gene expression in response to endogenous and exogenous ligands (Barish *et al*, 2006; Desvergne *et al*, 2006; Feige *et al*, 2006). The PPAR family consists of three members, PPARα, PPARβ/δ and PPARγ, whose major physiological functions are associated with the regulation of intermediary metabolism. All PPARs are activated by fatty acids and some derivatives, but there are no known subtype-specific, high-affinity endogenous ligands, suggesting that PPARs act as intracellular lipid sensors (Forman *et al*, 1997; Desvergne *et al*, 2006). However, PPARs are highly relevant drug targets, which has led to the development of several synthetic drug agonists showing increased subtype selectivity and high-affinity binding (Peraza *et al*, 2006). PPARs form obligatory heterodimers with the nuclear receptor RXRα on PPAR response elements (PPREs) in their target genes resulting in transcriptional activation. PPARs can also repress genes by directly interacting with specific transcription factors and recruiting corepressor proteins (Lee *et al*, 2003).

It has recently been shown that PPARβ has a critical role in modulating skeletal muscle lipid catabolism, glucose homeostasis and macrophage activation (Barish *et al*, 2006; Desvergne *et al*, 2006). Thus, PPARβ represents a new potential drug target for the treatment of major human diseases such as obesity, metabolic syndrome, inflammation and arteriosclerosis. Intriguingly, PPARβ also promotes cellular differentiation and inhibits proliferation and apoptosis of different cell types (Tan *et al*, 2001; Schmuth *et al*, 2004; Kim *et al*, 2006; Nadra *et al*, 2006; Varnat *et al*, 2006). *Pparb*-null mice exhibit a defect in wound healing, and increased keratinocyte proliferation occurs in the skin of *Pparb*-null mice treated with a tumor promoter (Peters *et al*, 2000; Michalik *et al*, 2001). Furthermore, ligand activation of PPARβ selectively stimulates keratinocyte differentiation and inhibits proliferation (Kim *et al*, 2006), concomitant with a ubiquitin-mediated downregulation of protein kinase C-α and MAP kinase signaling (Kim *et al*, 2005).

Consistent with its function in differentiation and proliferation, PPARβ plays a role in intestinal tumorigenesis. In the human colon cancer cell line HCT116, *Pparb* disruption has been reported to result in a loss of tumorigenicity (Park *et al*, 2001). However, in intestinal tumor mouse models, PPARβ affected adenoma growth to a variable extent in different studies (Barak *et al*, 2002; Gupta *et al*, 2004; Harman *et al*, 2004; Reed *et al*, 2004; Marin *et al*, 2006). Both, the homozygous deletion of *Pparb* (Harman *et al*, 2004; Reed *et al*, 2004) and the pharmacological activation of PPARβ (Gupta *et al*, 2004; Marin *et al*, 2006), have been shown to exert subtle, although statistically significant effects on adenoma growth, but the precise function of PPARβ in intestinal tumor cells remains controversial (Burdick *et al*, 2006).

None of the mouse studies performed to date addressed the issue as to whether PPARβ might play a role in the cells of the tumor stoma, that is, host cells recruited by the tumor, such as endothelial cells (ECs), fibroblasts and macrophages

*Corresponding author. Institute of Molecular Biology and Tumor Research (IMT), Philipps-University, Emil-Mannkopff-Strasse 2, Marburg 35032, Germany. Tel.: +49 6421 2866236; Fax: +49 6421 2868923; E-mail: rmueller@imt.uni-marburg.de
[6]These authors contributed equally to this work

Received: 25 January 2007; accepted: 29 June 2007; published online: 19 July 2007

(Bissell and Radisky, 2001). In the present study, we have specifically addressed this question.

Results

Inhibition of tumor growth in Pparb$^{-/-}$ mice

We first asked whether the genetic status of *Pparb* in host cells would affect the growth of transplanted syngeneic tumor cells. *Pparb*$^{-/-}$ mice have been described previously and shown to lack PPARβ protein in all tissues analyzed (Peters *et al*, 2000; Harman *et al*, 2004). This was confirmed in the present study for fibroblasts and ECs as typical stromal cell types (Supplementary Figure S1). Lewis lung carcinoma (LLC1) cells were inoculated subcutaneously into *Pparb*$^{+/+}$ and *Pparb*$^{-/-}$ mice. Rapid and progressive tumor growth was observed in all *Pparb*$^{+/+}$ mice ($n=15$), invariably leading to death within 24 days. Tumor growth in *Pparb*$^{-/-}$ mice ($n=11$) was initially indistinguishable from *Pparb*$^{+/+}$ mice, but halted after approximately 14 days, resulting in 100% survival 32 days after tumor cell implantation, and 90.9% survival after >6 months (Figure 1A; Table I). We also observed a dramatic inhibition of tumor growth with the B16F1 melanoma model (Figure 1B). While the inoculated *Pparb*$^{+/+}$ mice invariably succumbed to the B16F1 tumors within 14 days, all *Pparb*$^{-/-}$ mice showed a clear retardation of tumor growth (Figure 1B; $n=8$), and exhibited a survival rate of 100% on day 24.

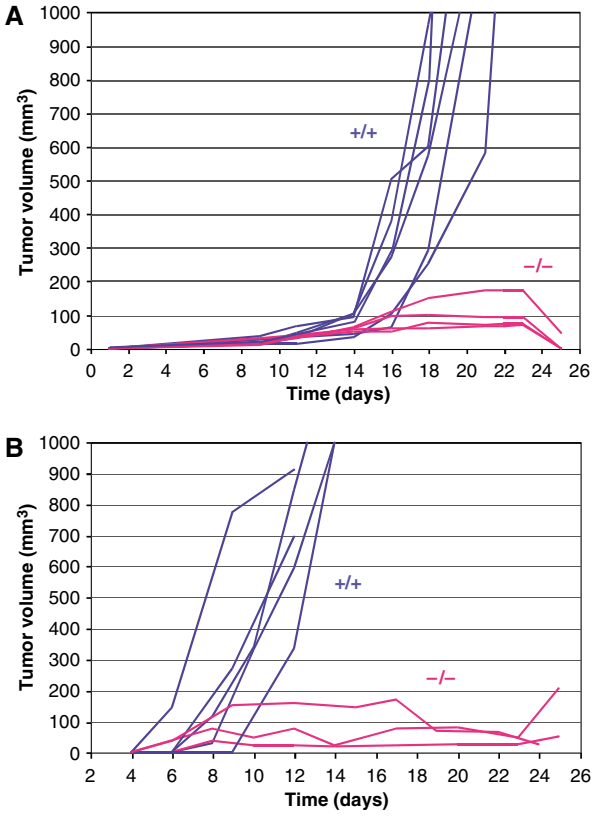

Figure 1 Blockade of syngeneic tumor growth in *Pparb*$^{-/-}$ mice. *Pparb*$^{+/+}$ and *Pparb*$^{-/-}$ mice were inoculated subcutaneously with LLC1 (**A**) or B16F1 cells (**B**), and tumor sizes were determined at the times indicated. Blue lines: *Pparb*$^{+/+}$ mice; red lines: *Pparb*$^{-/-}$ mice. Mice were killed when the calculated tumor volume exceeded 1000 mm^3, or when tumors became necrotic. Panel A shows one of the two independent experiments summarized in Table I.

Abnormal microvascular structures in Pparb$^{-/-}$ mice

Blood vessels in LLC1 tumors were visualized by immunohistochemistry using an antibody directed against aquaporin-1 (AQP-1), a specific marker for ECs and erythrocytes (Saadoun *et al*, 2005). Microvessels with a thin lining of ECs and an open lumen with erythrocytes were readily detected in LLC1 tumors from *Pparb*$^{+/+}$ mice (Figure 2A). In contrast, microvessels with a normal appearance were rare in LLC1 tumors from *Pparb*$^{-/-}$ mice, where ECs were found mainly in highly abnormal structures lacking a lumen (Figure 2A). These presumably defective microvessels were frequently located in areas of extensive tumor necrosis, as exemplified in Figure 2A by the cellular debris seen around the abnormal vascular structures. Importantly, immunostaining with antibodies for macrophages, neutrophils or lymphocytes (Supplementary data) revealed only very few cells in tumors of either genotype, clearly suggesting that inflammatory and immune cells did not play an essential role in supporting or restraining LLC1 tumor growth (data not shown).

Surprisingly, a quantitative evaluation revealed a threefold higher microvascular density in LLC1 tumors from *Pparb*$^{-/-}$ mice (Figure 2B, left panel; $n=8$; $P=0.010$). However, while 76% of these structures represented morphologically normal microvessels in *Pparb*$^{+/+}$ mice, this was reduced to 11.8% in *Pparb*$^{-/-}$ mice (Figure 2B, right panel; $n=8$; $P=0.010$). These observations suggest that an abnormal organization rather than a lack of ECs underlies the abundance of abnormal microvessels in *Pparb*$^{-/-}$ mice.

Diminished blood flow in LLC1 tumors in Pparb$^{-/-}$ mice

Functional evidence for a tumor vascularization defect in *Pparb*$^{-/-}$ mice was obtained by dynamic contrast-enhanced magnetic resonance imaging (DCE-MRI) (Choyke *et al*, 2003; Kiessling *et al*, 2003). Contrast medium (diethylenetriamine pentaacetic acid; Gd-DTPA) was injected into three *PPARb*$^{+/+}$ and three *PPARb*$^{-/-}$ mice and tumor accumulation was monitored over 9 min. All tumors had a similar volume at the beginning of the analysis (5.3 ± 1.3 mm^3; day 0 in Figure 3B). Measurements were repeated after 2 and 6 days with the identical animals. Tumors in *Pparb*$^{+/+}$ mice showed continuous progression, reaching sizes of >1000 mm^3, whereas tumors in *Pparb*$^{-/-}$ mice grew much slower followed by a partial regression. Kinetic analysis of

Table I Growth of LLC1 tumors in syngeneic *Pparb*$^{+/+}$ and *Pparb*$^{-/-}$ mice

Genotype	Tumor volume (mm^3) Day 9	Doubling time (days) Day 9–14	Doubling time (days) Day 14–21	Survival (*n*) >Day 24
Pparb$^{+/+}$	6.4 ± 5.4[a]	2.3 ± 1.4[a]	1.4 ± 0.2[b]	0/15
Pparb$^{-/-}$	7.5 ± 4.9[a]	2.7 ± 1.3[a]	>13[b]	11/11[c]

[a]Differences between *Pparb*$^{+/+}$ and *Pparb*$^{-/-}$ mice not significant (*t*-test; $P>0.6$).
[b]Differences highly significant ($P=0.03$).
[c]Ten tumors regressed completely, one mouse was killed after 33 days ($P<0.0001$). Data are obtained from two separate experiments ($n=26$).

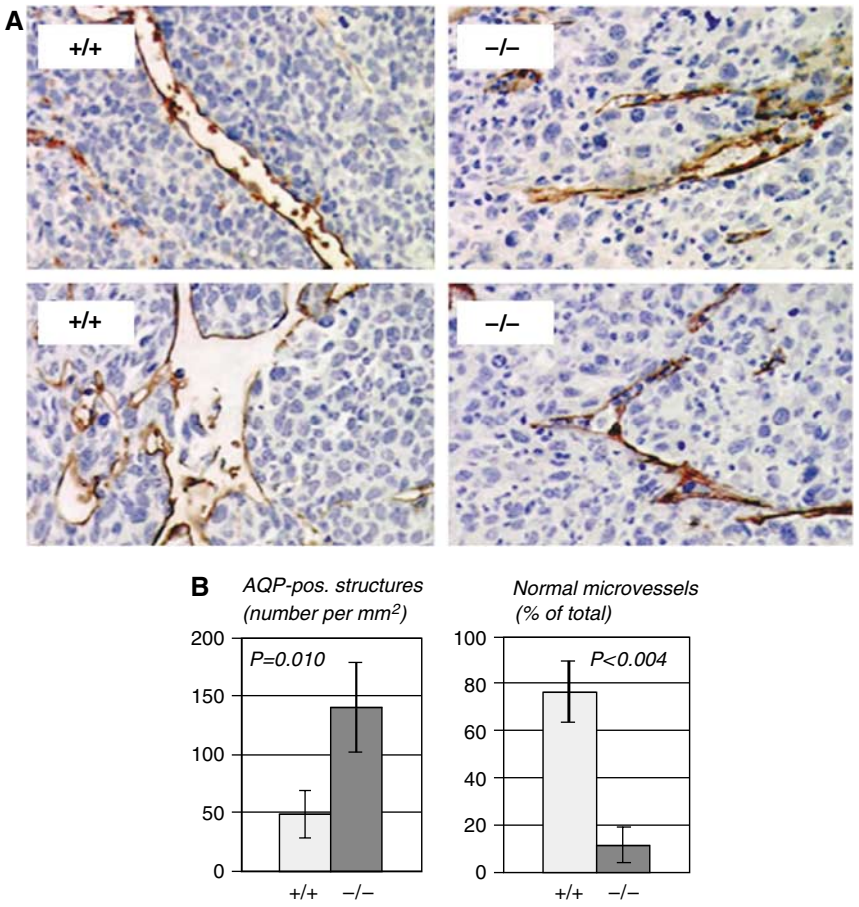

Figure 2 Immunohistological analysis of ECs in LLC1 tumors. (**A**) AQP-1 immunostaining (Saadoun *et al*, 2005) of ECs and blood vessels in subcutaneous LLC1 tumors 14 days after inoculation into *Pparb*$^{+/+}$ and *Pparb*$^{-/-}$ mice (brown stain). Microscopic magnification, × 50. Areas of tumor cell necrosis are seen in the vicinity of aberrant vascular structures in *Pparb*$^{-/-}$ mice (debris). These differences between *Pparb*$^{+/+}$ and *Pparb*$^{-/-}$ mice were independent of tumor size and were confirmed by using antibodies against von Willebrand factor or CD34 (data not shown). (**B**) Quantitative evaluation of AQP-1-positive structures in LLC1 tumors from *Pparb*$^{+/+}$ and *Pparb*$^{-/-}$ mice. The indicated *P*-values were determined by *t*-test.

Gd-DTPA accumulation in tumors revealed a rapid and high amplitude wash-in followed by a clearly discernible wash-out phase in *Pparb*$^{+/+}$ mice at all time points analyzed (Figure 3B), indicative of functional vascularization (Choyke *et al*, 2003; Kiessling *et al*, 2003). In contrast, *Pparb*$^{-/-}$ mice showed a progressive delay of wash-in and no wash-out phase, indicating an obstructed blood flow into and through the tumor tissue (Figure 3B). Analysis of dynamic Gd-DTPA within individual tumors showed a relatively even distribution in tumors in *Pparb*$^{+/+}$ mice, whereas large regions of decreased accumulation were seen in *Pparb*$^{-/-}$ mice, especially in the regressing tumors (green/blue areas in Figure 3A) next to regions showing rapid accumulation (red areas in Figure 3A). These observations are consistent with the histological analyses showing that a large fraction of tumor microvessels is abnormal in *Pparb*$^{-/-}$ mice.

Endothelial hyperplasia in LLC1 tumors in Pparb$^{-/-}$ *mice*

To examine the cellular basis underlying the observed vascular phenotype we performed double immunostaining for AQP-1 and proliferating cell nuclear antigen (PCNA). A considerably higher number of PCNA-positive cells in tumors was found in *Pparb*$^{-/-}$ mice as compared with *Pparb*$^{+/+}$ mice (38.7 versus 16.6%; Figure 4A; $n=8$; $P=0.010$). Consistent with these *in vivo* observations, we found that the proliferation of primary aortic ECs from *Pparb*$^{-/-}$ mice was enhanced compared to *Pparb*$^{+/+}$ cells cultured on a tumor basement membrane-derived matrix (matrigel), in the presence of pro-angiogenic growth factors (Figure 4B).

Microvessels in *Pparb*$^{-/-}$ mice were typically lined by morphologically less mature ECs frequently protruding into the vessel lumen reminiscent of endothelial hyperplasia. These vessels were surrounded by rings of cells strongly expressing the myofibroblast/pericyte marker smooth muscle α-actin (SMA) (Bissell and Radisky, 2001) (Figure 5A and B). Hyperplastic tumor endothelial structures were also found in the absence of adjacent perivascular SMA expressing cells, indicating that the occurrence of these SMA-positive cells is not a prerequisite for vascular dysfunction.

Immature, hyperproliferative ECs in matrigel plugs in Pparb$^{-/-}$ *mice*

To study the role of PPARβ in an independent *in vivo* angiogenesis assay, we performed matrigel plug assays (Ley *et al*, 2004) using prostaglandin E_2 (PGE_2) and basic fibroblast growth factor (FGF-2) as angiogenic stimuli. These subcutaneous plugs became rapidly invaded by

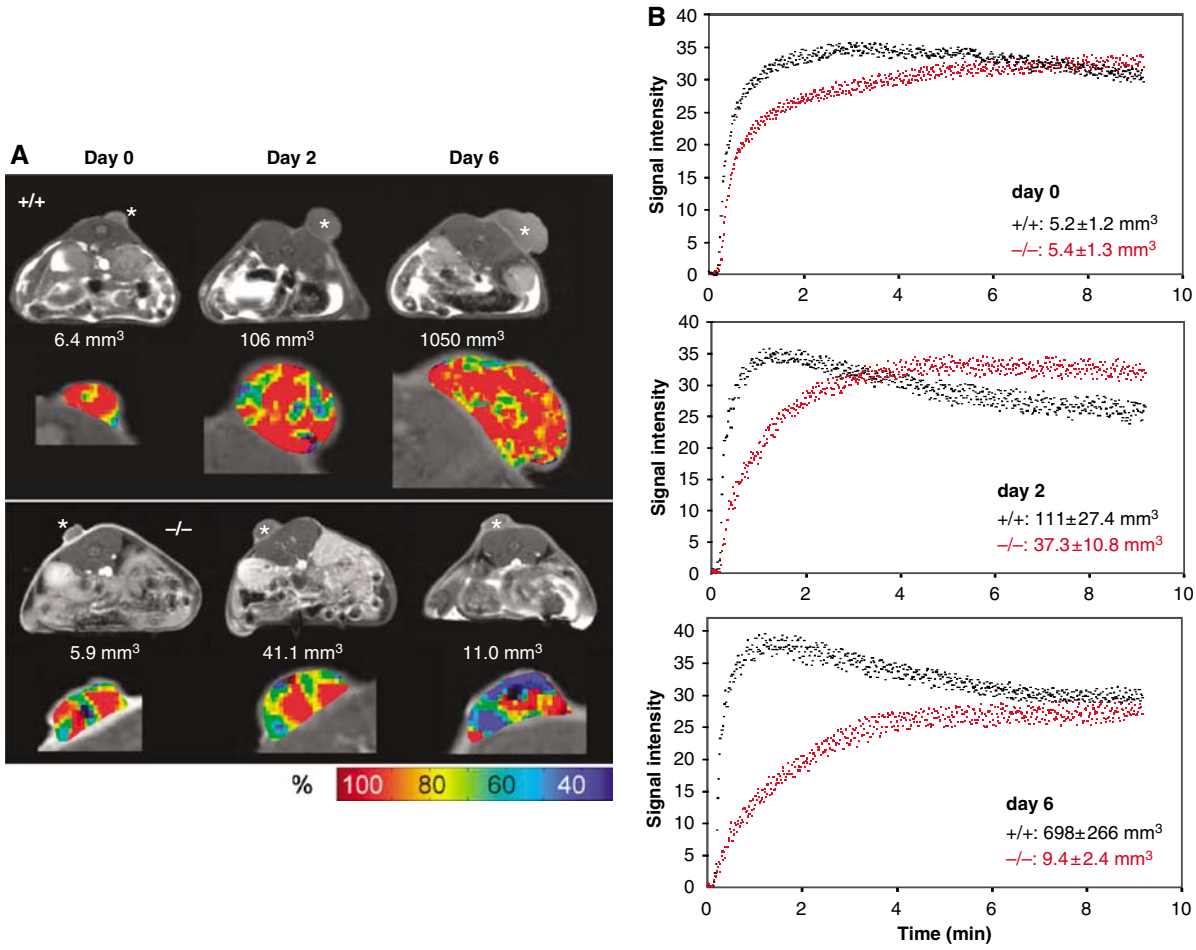

Figure 3 Magnetic resonance image analysis of LLC1 tumors. (**A**) DCE-MRI analysis of LLC1 tumors in *PPARb*$^{+/+}$ and *PPARb*$^{-/-}$ mice at different stages of tumor development. *Pparb*$^{+/+}$ and *Pparb*$^{-/-}$ mice harboring tumors of similar size were selected, and DCE-MRI analyses were performed at the beginning of the experiment (designated day 0) and after 2 and 6 days. During this time *Pparb*$^{+/+}$ mice showed progressive growth, while tumors in *Pparb*$^{-/-}$ mice regressed after an initial growth phase. The respective tumor volumes are indicated in the figure. Top rows (gray scale): MRI images obtained before administration of contrast medium. *s.c. LLC1 tumors. Bottom rows (pseudo-color images): DCE-MRI analysis of tumors 100 s. after i.v. injection of contrast medium. Red areas represent regions of maximum enhancement of signal intensities based on shortened T1 relaxation times caused by contrast medium accumulation in the vascular and extravascular extracellular space. Green/blue areas represent regions of lower signal intensity enhancement indicating decreased influx of contrast medium (see scale for color codes). (**B**) Quantification of DCE-MRI analysis of tumors in *PPARb*$^{+/+}$ (black dots) and *PPARb*$^{-/-}$ (red dots) mice performed as in panel A. The data show the enhancement of signal intensities (shortened T1 relaxation times; arbitrary units) during the first 9 min after the injection of contrast medium. Data represent absolute values. Tumor volumes are shown as means±s.d. Three mice of each genotype were analyzed.

AQP-1-positive cells (Figure 6A and B). In *Pparb*$^{+/+}$ mice, the invading cells aligned within 3 days to form network-like structures consisting of elongated cells connected by dendritic processes (Figure 6A, left panel). These ordered structures were largely absent from matrigel plugs in *Pparb*$^{-/-}$ mice (Figure 6A, right panel). While morphologically mature cells (flat, elongated cells with processes) represented 39.6±10.0% of cells in microvascular structures in *Pparb*$^{+/+}$ mice, the corresponding value was 13.9±2.3% for *Pparb*$^{-/-}$ mice (Figure 6C, left panel). Matrigel plugs in *Pparb*$^{+/+}$ mice also contained more advanced structures lined by elongated ECs (Figure 6B, left panel), whereas morphologically aberrant cells protruding into the lumen were seen in *Pparb*$^{-/-}$ mice (Figure 6B, right panel). Consistent with the hyperproliferation of tumor ECs shown above, we found a significantly higher proportion of PCNA-positive cells in matrigel plugs from *Pparb*$^{-/-}$ mice (37.2±0.7%), compared with *Pparb*$^{+/+}$ mice (14.8±0.8%; Figure 6C, right panel).

Consistent with its essential role in tumor vascularization, we also found that *Pparb* is the predominant *Ppar* subtype expressed in angiogenic matrigel plugs, in mouse ECs isolated from subcutaneous tumors (Supplementary Figure S2), and in tumor ECs from human lung carcinomas (Supplementary Figure S3), and that it is inducible by angiogenic growth factors in ECs *in vitro* (Supplementary Figure S4).

Restoration of PPARβ expression triggers microvessel maturation

To determine whether re-expression of PPARβ in matrigel-invading cells would restore normal vascularization in *Pparb*$^{-/-}$ mice, we established a syngeneic fibroblast producer line (3Fb-p cells) expressing FLAG-PPARβ and helper retroviruses (Supplementary Figure S1). Matrigel plugs containing these cells were used with the same experimental design described above. Immunohistological analysis of matrigel plugs 3 days post-implantation showed FLAG-positive

implanted fibroblasts (occurring in small colonies) and FLAG-positive host ECs, whereas the inclusion of transduced control cells either lacking the FLAG-PPARβ retrovirus (Lpcx-p cells) or the helper virus (3Fb-np non-producer cells) did not yield any FLAG-specific host cell staining (Figure 7A). Concomitant with this viral spread and re-expression of PPARβ in the invading host cells, we observed the appearance of vessels containing erythrocytes lined by morphologically normal ECs, whereas in the presence of either control cell line, microvascular structures remained abnormal and were devoid of red blood cells without exception (Figure 7B and C). This observation provides additional strong evidence for a role of PPARβ in promoting vascularization in a mouse model of tumor angiogenesis.

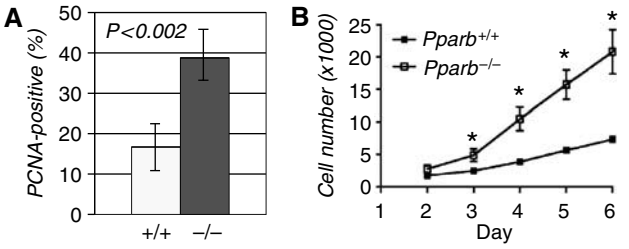

Figure 4 Effect of PPARβ on endothelial cell proliferation. (**A**) Proliferative index of ECs in LLC1 tumors from *Pparb*$^{+/+}$ and *Pparb*$^{-/-}$ mice determined as the PCNA-positive fraction (%) of AQP-1-positive cells. The indicated *P*-values were determined by *t*-test. (**B**) Proliferation of primary aortic ECs from *Pparb*$^{+/+}$ and *Pparb*$^{-/-}$ mice. Cells were seeded in tissue culture plates and cell numbers were determined for up to 6 days. Cells isolated from each mouse were kept separate and data represent the mean result obtained from 2–3 mice per genotype. *Statistically significant from *Pparb*$^{+/+}$ (*t*-test, $P \leqslant 0.05$). We also observed differentiation of aortic ECs from mice of both genotypes into tube-like structures in the matrigel. While differentiation of *Pparb*$^{-/-}$ EC cells seemed to be retarded compared with *Pparb*$^{+/+}$, cells we were unable to demonstrate definitive morphological differences (not shown).

Altered gene expression in matrigel-invading cells in Pparb$^{-/-}$ *mice*

Cells from matrigel plugs were analyzed by qPCR for the expression of EC, fibroblast and macrophage marker genes (*Aqp-1*, *Cd105*, *vimentin*, *Cd14*, *Cd68*, *F4/80*). No significant differences were detectable between *Pparb*$^{+/+}$ and *Pparb*$^{-/-}$ samples (Supplementary Figure S5, and data not shown), indicating a very similar composition of cell types. To identify angiogenesis-associated PPARβ target genes, we first analyzed a number of known genes (including all VEGFs, Flk-1, Angiopoietin-1/2, Tie-1/2, VE-cadherin), but could not detect any significant differences among *Pparb*$^{+/+}$ and *Pparb*$^{-/-}$ samples (data not shown). We therefore compared the gene expression profile of both samples by microarray analysis (ArrayExpress, E-MEXP-983). In *Pparb*$^{+/+}$ cells, 39 genes were found to be expressed at higher levels, while 27 genes showed lower expression (cut-off 1.7-fold; Supplementary Table S1). As expected, several of these genes encode proteins with functions in lipid metabolism that have previously been identified as PPAR target genes, that is, fatty acid binding protein 4 (*Fabp4* gene), acyl-CoA dehydrogenase (long-chain; *Acadl* gene), stearoyl-CoA desaturase 1 (*Scd1* gene) and the CD36 fatty acid translocase/thrombospondin receptor (*Cd36* gene) (see references in

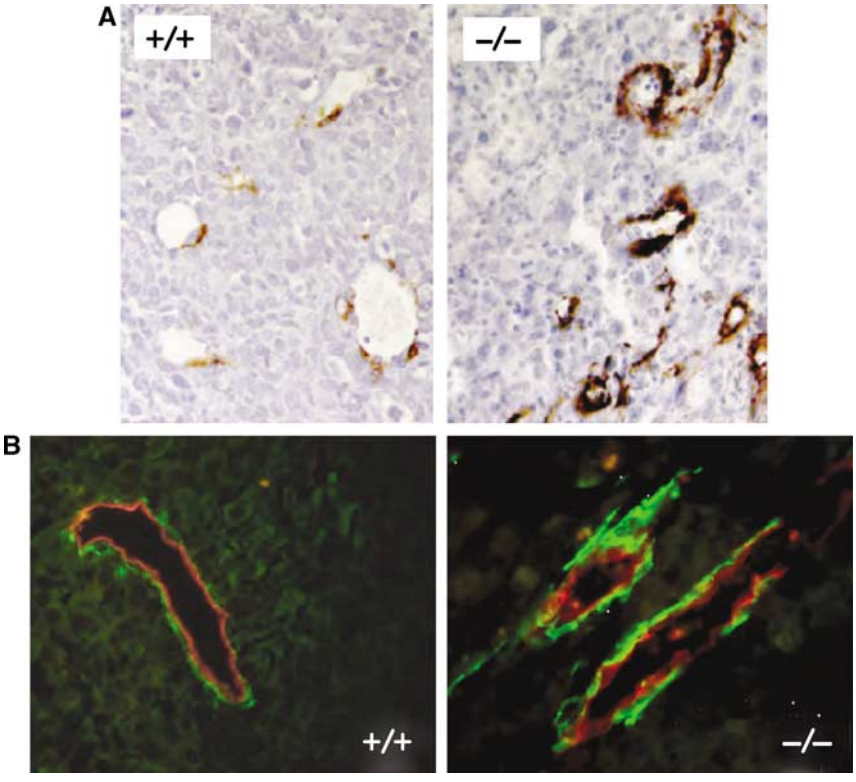

Figure 5 Immunostaining of SMA in LLC tumors. (**A**) SMA immunostaining of LLC1 tumors from *Pparb*$^{+/+}$ and *Pparb*$^{-/-}$ mice. Microscopic magnification, ×50. (**B**) AQP-1/SMA double immunofluorescence of LLC1 tumors from *Pparb*$^{+/+}$ and *Pparb*$^{-/-}$ mice. Red, AQP-1, green: SMA. Microscopic magnification, ×50.

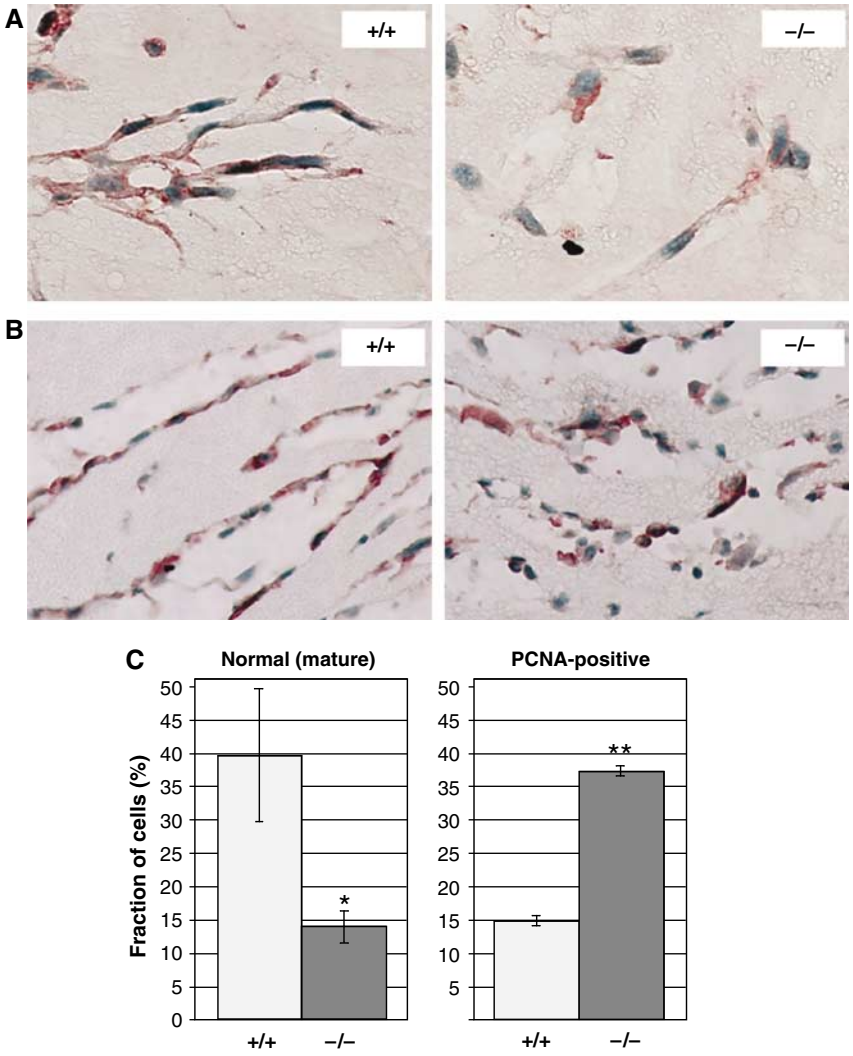

Figure 6 Analysis of PPARβ function in angiogenic ECs *in vivo*. (**A, B**) AQP-1 staining of formalin-fixed and paraffin-embedded of bFGF/PGE_2 containing matrigel plugs (Ley *et al*, 2004) 3 days after s.c. implantation into $Pparb^{+/+}$ and $Pparb^{-/-}$ mice. Microscopic magnification, ×100 (A) and ×50 (B). The images show the formation of network-like structures in $Pparb^{+/+}$ mice. Panel B shows more advanced stages of microvessel formation. Very similar results were obtained with fluorescently labeled isolectin B4 (data not shown), a selective label for mouse blood vessels (Kawamoto *et al*, 2003). (**C**) Quantitative evaluation of morphologically mature (left panel) and PCNA-positive (right panel) ECs in matrigel plugs. ***Statistically significant difference to $Pparb^{+/+}$ (*t*-test, $P \leqslant 0.05$).

Supplementary Table S1). Differential expression in $Pparb^{+/+}$ and $Pparb^{-/-}$ cells was verified by qPCR for a subset of genes, with a focus on those coding for regulatory proteins (Supplementary Figure S5). Of these genes, *Cdkn1c* is of particular interest due to the established direct role of its encoded protein $p57^{KIP2}$ as a negative regulator of the cell cycle (Lee *et al*, 1995). We also analyzed the expression of genes coding for other CDK inhibitors (*Cdkn1a, Cdkn1b, Cdkn2a, Cdkn2b, Cdkn2c*), but were unable to detect significant differences between $Pparb^{+/+}$ and $Pparb^{-/-}$ mice (Figure 8A, and data not shown). Importantly, we found readily detectable levels of *Cdkn1c* expression in ECs isolated from four independent samples of primary human lung carcinomas (Supplementary Figure S3), which is consistent with a potential role in tumor vascularization. We therefore focused on *Cdkn1c* in all subsequent experiments.

Confirmation of Cdkn1c as a PPARβ target gene

To obtain independent evidence that the *Cdkn1c* gene is regulated by PPARβ, we used fibroblasts established from a mouse strain with a floxed *Pparb* allele (Barak *et al*, 2002). Figure 9 shows that the expression of *Cdkn1c* was reduced ~2.5-fold after infection with a Cre expressing retrovirus (Li *et al*, 1997) relative to control virus infected cells. As a positive control, we included the known PPAR target gene *Pdk4* (coding for pyruvate dehydrogenase kinase-4) (Kitz Kramer *et al*, 2007), which also showed the expected reduction (~8-fold) in the PPARb-deleted cells.

We next investigated whether the change in *Cdkn1c* expression in PPARβ-deficient cells could be 'rescued' by retrovirus-mediated re-expression of PPARβ. As shown in Figure 8C, $Pparb^{-/-}$ fibroblasts infected with the PPARβ retrovirus expressed the *Cdkn1c* gene at ~8-fold elevated levels. As expected, the bona fide PPAR target genes *Pdk4* and *Fapb4* also showed a clear upregulation.

We also studied the inducibility of *Cdkn1c* by the synthetic PPARβ-selective agonist, GW501516 (1 μM), in human umbilical vein ECs (HuVECs). In this setting, the *Pdk4* gene was rapidly induced within 4 h by a factor of ~4, as expected (Figure 8D). Likewise, *Cdkn1c* expression increased more

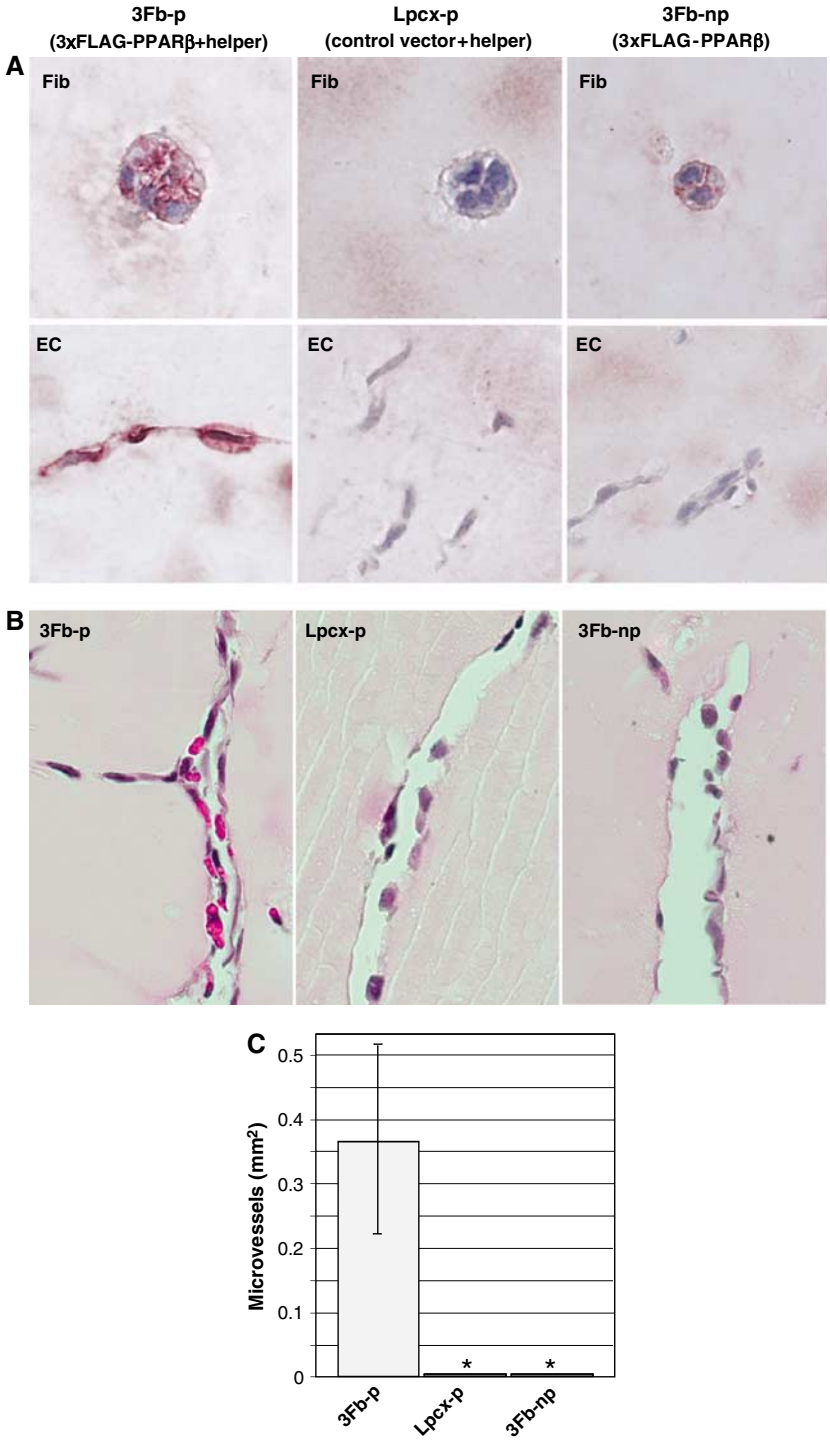

Figure 7 Promotion of microvessel maturation in *Pparb*$^{-/-}$ mice by PPARβ expressing retroviruses. (**A**) Immunohistochemical staining for PPARβ of matrigel plugs containing retroviral producer cells. *Pparb*$^{-/-}$ fibroblasts were infected with a replication-deficient retrovirus expressing an fully functional N-terminally triple-FLAG-tagged PPARβ. A non-producer clone (3Fb1 cells) showing FLAG expression in nearly 100% of the population and a control line harboring empty pLPCX vector (Lpcx cells) were chosen for subsequent studies. From both cell lines we generated virus-producer lines (3Fb1-p and Lpcx-p, respectively) by super-infection with an Mo-MuLV-based helper virus. These producer cells were included in matrigel plugs containing PGE_2 and FGF-2. Immunohistological analysis of matrigel plugs 3 days post-implantation showed FLAG-positive fibroblasts (occurring in small colonies; 'Fib' in the figure above) and FLAG-positive, AQP-1-positive cells ('EC' in the figure above) in the presence of 3Fb-p cells (left); FLAG-negative implanted fibroblasts and FLAG-negative host cells in control Lpcx-p containing plugs (middle); and FLAG-positive fibroblasts and FLAG-negative host cells in non-producer 3Fb-np containing plugs (right). (**B**) Effect of restored PPARβ expression on microvessel formation in FGF-2/PGE_2 matrigel plugs in *Pparb*$^{-/-}$ mice. Morphologically mature erythrocyte containing microvessels were induced by 3Fb-p cells (left panel), but not by control producer cells (Lpcx-p) or non-producer 3Fb-np cells. The pictures show HE-stained paraffin sections. Microscopic magnification, $\times 50$. (**C**) Quantitative evaluation of morphologically normal microvessels in the matrigel plugs shown in panel B. *Statistically significant difference to 3Fb-p (*t*-test, $P \leqslant 0.05$).

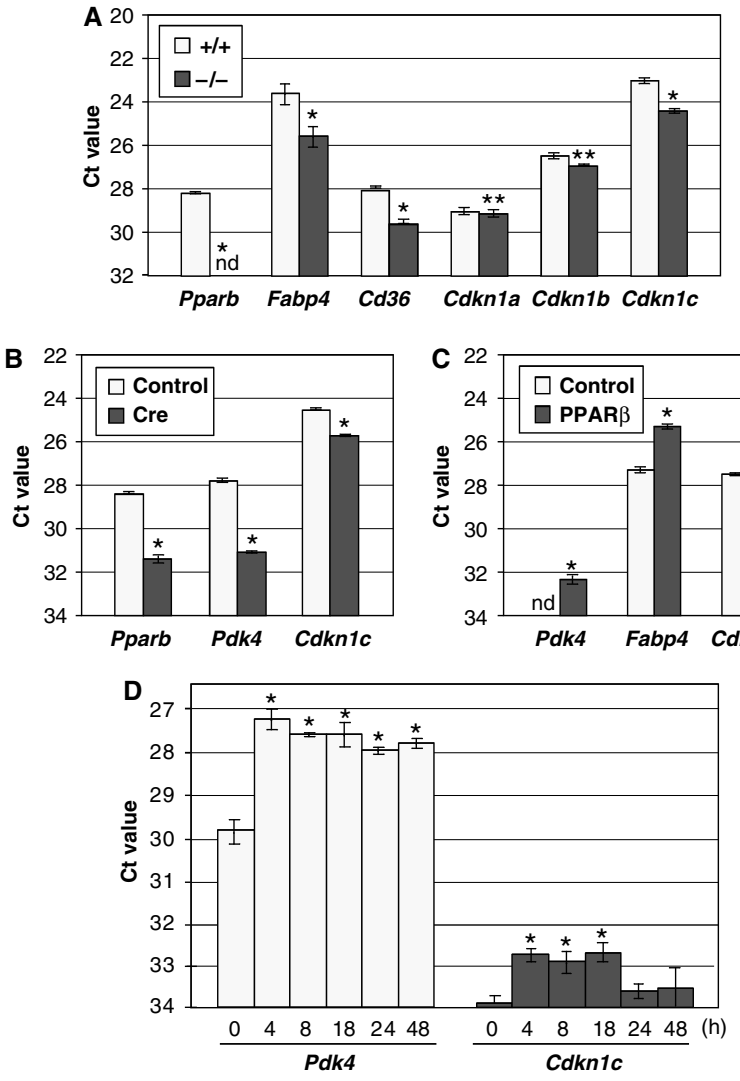

Figure 8 Regulation of *Cdkn1c* expression by PPARβ. (**A**) Gene expression patterns of matrigel-invading cells from $Pparb^{+/+}$ and $Pparb^{-/-}$ mice 3 days after implantation were analyzed by qPCR. Data represent the mean values for three individual plugs from each genotype (±s.d.) normalized to *Arp0* (Ct = 17). (**B**) Effect of Cre-mediated *Pparb* disruption on the *Cdkn1c* gene. Lung fibroblasts with floxed *PPARb* (LF-Flox-PPARb cells) were infected with a Cre retrovirus (Li *et al*, 1997) or with control virus (pBABE), and the isolated RNA was analyzed by qPCR for expression of the genes indicated. *Pdk4* and *Fabp4* are known PPAR target genes and were included as positive controls. Values represent Ct values (averages of triplicates ± s.d.) normalized to *Arp0* (Ct = 18). The *Pparb* primers used in this panel recognize only the floxed allele. (**C**) Effect of PPARβ re-expression in $Pparb^{-/-}$ cells on *Cdkn1c* and known PPAR target gene. Expression patterns of FLAG-PPARβ expressing 3Fb and control Lpcx cells were compared by qPCR. Values represent Ct values (averages of triplicates ± s.d.) normalized to *L27* (Ct = 17). (**D**) Induction of the *Cdkn1c* gene by 1 μM GW501516 in HUVECs. Cells were treated for the indicated times, RNA was isolated and analyzed by qPCR. *Pdk4* was included as a known PPAR target gene (positive control). Values represent Ct values (averages of triplicates ± s.d.) normalized to *Arp0* (Ct = 17). *Values significantly different ($P < 0.05$) between $Pparb^{-/-}$ cells $Pparb^{-/-}$ cells (panels A–C) or from time = 0 (panel D). **Differences not significant ($P > 0.05$). nd: not detectable.

than two-fold at 4 h post-treatment, decreasing to near basal levels at 24 h, confirming that *Cdkn1c* is a PPARβ target gene.

Inspection of the mouse *Cdkn1c* upstream sequence revealed two motifs at positions −1670 and −710 fitting the PPRE consensus sequence (Supplementary Figure S6, top panel). We cloned a 1.7-kb *Cdkn1c* promoter fragment harboring these elements, in front of a luciferase reporter gene, and analyzed this construct in mouse 2H11 ECs. We observed a 1.8-fold induction after cotransfection of PPARβ and RxRα expression plasmids, which was further increased by the PPARβ agonist GW501516 to 2.6-fold (Supplementary Figure S6). These data clearly confirm that *Cdkn1c* induction by PPARβ is mediated by a transcriptional mechanism.

PPARβ-mediated inhibition of cell proliferation involves p57^{KIP2}

We next sought to investigate the growth inhibitory effect of PPARβ on a stroma cell type in further detail using a cell culture model. As shown in Figure 9A, infection of $Pparb^{-/-}$ cells with FLAG-PPARβ retrovirus resulted in a strong inhibition of cell proliferation compared with control virus infected cells (3F1.13 versus Lpcx cells). This growth inhibitory effect of PPARβ imposes a selection pressure against PPARβ expressing cells. Thus, the continuous passaging of 3F1.13 cells resulted in a clear decrease in PPARb expression (subline 3F1.24; Figure 9B), which correlated with an increase in proliferation (Figure 9A). However, 3F1.24 cells still prolifer-

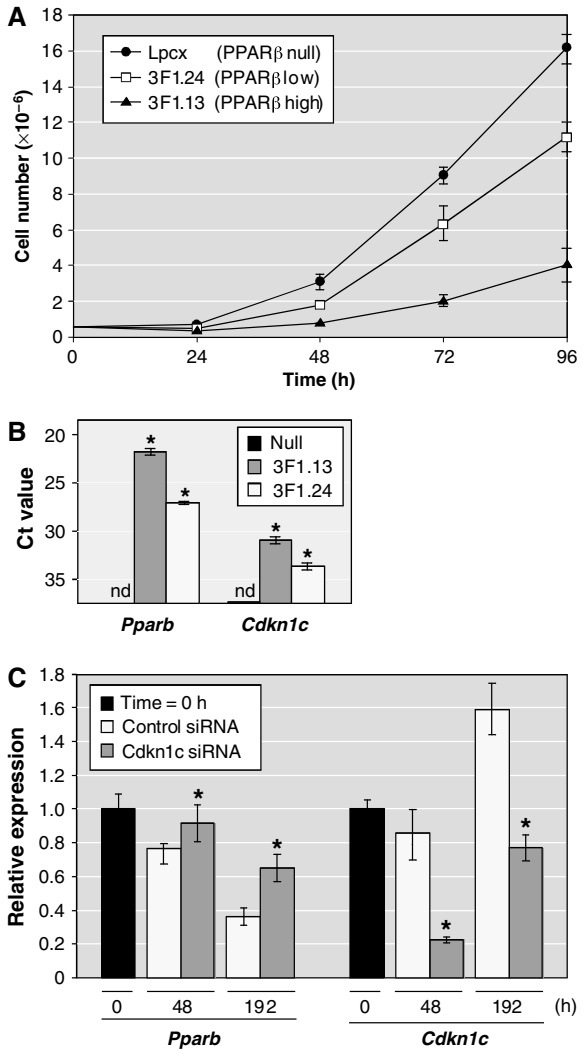

Figure 9 PPARβ mediated inhibition of cell proliferation involves $p57^{KIP2}$. (**A**) Growth curves of cells expressing different levels of PPARβ as indicated in the figure. Lpcx cells: *Pparb*$^{-/-}$ fibroblasts infected with a control retrovirus (pLPCX); 3F1.13 and 3F1.24 cells: FLAG-PPARβ retrovirus infected *Pparb*$^{-/-}$ fibroblasts. 3F1.24 cells are a derivative of 3F1.13 cells. Cells were seeded at a density of 0.5×10^5 cells/3 cm dish and triplicates were counted every 24 h for 96 h. Data represent the mean of triplicates (±s.d.). (**B**) *Pparb* and *Cdkn1c* expression (qPCR) in the cell lines used in A. Values represent Ct values (averages of triplicates±s.d.) normalized to *L27* (Ct = 19). *Values significantly different from Lpcx versus 3F1.13 or 3F1.24 cells ($P < 0.05$). (**C**) Effect of *Cdkn1c* knockdown on PPARβ-mediated growth inhibition. *Pparb*$^{-/-}$ cells infected with a FLAG-PPARβ retrovirus (as in A) were subcultured and transfected with siRNA 3-times over 144 h (Supplementary data). *Pparb* and *Cdkn1c* mRNA levels were measured at different time points up to 192 h after the first transfection. Values represent Ct values (averages of triplicates±s.d.) normalized to *Arp0* (Ct = 17). *Values significantly different from cells treated with control siRNA ($P < 0.05$). nd: not detectable.

ate more slowly than the *Pparb*$^{-/-}$ Lpcx cells, suggesting that a relatively low level of PPARβ suffices to attenuate cell proliferation (PPARb expression in 3F1.24 cells is similar to that in wild-type fibroblasts; data not shown). Importantly, both the level of PPARb and the extent of growth inhibition correlated with the level of *Cdkn1c* in the cell lines analyzed (Figure 9B).

To obtain direct evidence for a role of *Cdkn1c* in the inhibition of proliferation by PPARβ, we studied the effect of a *Cdkn1c* knockdown on the selection against PPARβ expressing cells in culture. *Pparb*$^{-/-}$ cells infected with a FLAG-PPARβ retrovirus were repeatedly passaged, and at each passage were treated with either a *Cdkn1c*-directed siRNA or an irrelevant control siRNA for a total period of 192 h. As shown in Figure 9C, *Cdkn1c* siRNA treatment reduced the level of *Cdkn1c* by 74% compared with the control siRNA at 48 h. *Cdkn1c* is a cell density-regulated gene (Samuelsson *et al*, 1999), which presumably caused the increased levels at 192 h in both *Cdkn1c*- and control siRNA-treated cells. Nevertheless, *Cdkn1c* levels were still 52% lower in the presence of *Cdkn1c* siRNA.

In control siRNA-treated cells, PPARb expression showed the expected rapid decline (76% after 48 h; 36% after 192 h), reflecting the selection pressure against PPARβ expressing cells. In contrast, *Cdkn1c* siRNA treatment resulted in significantly increased PPARb expression levels at both time points (92 and 65%, respectively). The clear loss of *Pparb* expression in the presence of *Cdkn1c* siRNA strongly suggests that *Cdkn1c* is a mediator of PPARβ-dependent inhibition of cell proliferation.

Discussion

Impaired tumor vascularization and tumor EC hyperplasia in Pparb$^{-/-}$ *mice*

A hallmark of tumors in *Pparb*$^{-/-}$ mice is the abundance of histologically highly abnormal microvessels showing a thickened endothelial lining and lacking a lumen, thus appearing dysfunctional (Figure 2). These alterations were associated with a striking increase in both tumor microvessel density and tumor EC proliferation (Figure 4A). Abnormal hyperproliferative endothelial structures were also seen in matrigel plugs (Figure 6), but never in any normal tissue of *Pparb*$^{-/-}$ mice. Thus, *Pparb*$^{-/-}$ ECs hyperproliferate under conditions resembling a tumor microenvironment. Concomitant with this hyperproliferation, tumor microvessels in *Pparb*$^{-/-}$ mice typically consist of immature ECs surrounded by perivascular cells expressing vast amounts of SMA (Figure 5), a condition characteristic of endothelial hyperplasia. That these histological abnormalities are functionally relevant, was demonstrated by kinetic DCE-MRI analysis of LLC1 tumors (Figure 3), which showed an obstructed tumor blood flow in *Pparb*$^{-/-}$ mice.

These observations strongly suggest that an abnormal organization caused by a hyperplastic response rather than a lack of ECs underlies the abundance of abnormal microvessels in *Pparb*$^{-/-}$ mice. However, the presence of a small fraction (11.8%) of morphologically normal tumor microvessels in *Pparb*$^{-/-}$ mice (Figure 2) obviously suffices to permit the formation of functional blood vessels, as indicated by the DCE-MRI analysis (Figure 3), which showed small but clearly detectable areas of blood flow even in regressing tumors in *Pparb*$^{-/-}$ mice. This small fraction of apparently functional tumor microvessels in *Pparb*$^{-/-}$ mice obviously suffices to permit tumor growth to volumes of $<100\,mm^3$ (Figure 1), which is clearly beyond the angiogenic threshold (Folkman, 2002), that is, the maximum size achievable by avascular tumors (approximately $4\,mm^3$). Together, these data indicate that tumor neoangiogenesis is principally functional in

Pparb$^{-/-}$ mice, but that a significant fraction of tumor microvessels is abnormal and dysfunctional, leading to an inhibition of tumor growth.

Even though a defect in angiogenesis has not been observed during normal development of *Pparb*$^{-/-}$ mice (Peters *et al*, 2000; Michalik *et al*, 2001; Barak *et al*, 2002; Nadra *et al*, 2006), our findings are in agreement with previous findings showing that PPARβ regulates terminal differentiation and has a negative regulatory role in the proliferation of different cell types, including keratinocytes (Tan *et al*, 2001; Schmuth *et al*, 2004; Kim *et al*, 2006; Burdick *et al*, 2007), trophoblast giant cells (Nadra *et al*, 2006) and intestinal epithelial cells (Marin *et al*, 2006; Varnat *et al*, 2006). This suggests that PPARβ is specifically required by tumor ECs to orchestrate their proliferation and differentiation in an environment, providing an abnormally rich source of growth factors and cytokines. This interpretation is consistent with our observations that the fraction of PCNA-positive matrigel-invading cells was 2.5-fold higher in *Pparb*$^{-/-}$ mice (Figure 6C), and that primary aortic ECs from *Pparb*$^{-/-}$ mice showed enhanced proliferation *in vitro* (Figure 4B). In both situations, ECs were exposed to high levels of soluble pro-angiogenic growth factors and a tumor basement membrane-derived matrix (matrigel).

A subtype-specific role for PPARβ in tumor ECs?

The three known PPAR subtypes have partially overlapping functions. Supplementary Figure S2 shows that in contrast to liver, *Pparb* is the predominant subtype in matrigel-invading cells. Likewise, in mouse ECs isolated from subcutaneous tumors (Supplementary Figure S2) and in ECs from primary human lung tumors (NSCLC) *Pparb* was the predominant subtype (Supplementary Figure S3). These observations point to a PPARβ-subtype specific function in tumor angiogenesis consistent with the phenotype observed in *Pparb*$^{-/-}$ mice. This is further supported by the induction of *Pparb* by angiogenic growth factors in cultured ECs (Supplementary Figure S4).

Altered Cdkn1c gene expression in Pparb$^{-/-}$ *stroma cells*

To address the molecular mechanisms underlying the observed phenotypic effects, we sought to identify genes that are regulated by *PPARβ in vivo* under conditions resembling tumor angiogenesis. Microarray and qPCR analysis of RNA from cells in matrigel plugs led to the identification of a set of genes that are differentially expressed in *Pparb*$^{+/+}$ and *Pparb*$^{-/-}$ mice (Supplementary Table S1; Figure 8A; Supplementary Figure S5). In view of the hyperplastic phenotype seen in *Pparb*$^{-/-}$, mice we were particularly interested in genes with a direct function in cell cycle regulation. The only gene fitting this criterion was *Cdkn1c* gene coding for the CDK inhibitor p57^{KIP2} (Lee *et al*, 1995). We therefore focused our further investigations on this gene and performed additional experiments to unequivocally confirm *Cdkn1c* as a PPARβ target gene. This was achieved by different strategies: (i) the Cre-mediated disruption of the *Pparb* gene in cultured fibroblasts resulted in the expected reduction of *Cdkn1c* expression (Figure 8B), (ii) the restoration of PPARβ expression in *Pparb*$^{-/-}$ fibroblasts led to a clear reactivation of *Cdkn1c* expression (Figure 8C), (iii) the treatment of primary ECs with the synthetic PPARβ agonist GW501516 rapidly induced the *Cdkn1c* gene (Figure 8D), and (iv) *in silico* analysis of the *Cdkn1c* upstream sequence revealed two potential PPREs, and consistent with this finding, we observed a clear induction of the *Cdkn1c* promoter by PPARβ/RxRα and GW501516 in transient transfection experiments (Supplementary Figure S6). The two latter observations (iii and iv) are characteristic of a direct PPAR target gene. A detailed analysis of the precise mechanisms underlying this regulation will be the subject of future studies.

Inhibition of cell proliferation by PPARβ

The inhibitory effect of PPARβ on stroma cell proliferation could be recapitulated in a cell culture model. Infection of fibroblasts isolated from *Pparb*$^{-/-}$ mice with a PPARβ expressing retrovirus resulted in a dose-dependent inhibition of cell proliferation and, upon continued passaging, in a selection against the PPARβ re-expressing cells. Two independent lines of evidence indicate that *Cdkn1c* is a PPARβ target gene that plays a pivotal role in the PPARβ-mediated attenuation of cell proliferation. First, there is good correlation between the re-expression of PPARβ, induction of *Cdkn1c* and the extent of growth inhibition (Figure 9A and B). Second, the selection against PPARβ expressing cells could be greatly diminished by an siRNA-mediated knockdown of *Cdkn1c* expression (Figure 9C). These results are consistent with the idea that the hyperproliferation of tumor ECs and matrigel-invading cells in *Pparb*$^{-/-}$ mice, results at least in part from a decrease in *Cdkn1c* expression. Consistent with this model, mice with a targeted disruption of the *Cdkn1c* gene have been reported to suffer from hyperplasia and an impairment of terminal differentiation in different tissues (Zhang *et al*, 1997).

Other potential PPARβ target genes

For two other genes downregulated in matrigel-invading cells from *Pparb*$^{-/-}$ mice, that is, *Cd36* and *Thbs2* (Supplementary Figure S5), an inhibitory role in angiogenesis has been established in previous studies (Lee *et al*, 1995; Armstrong and Bornstein, 2003). Thrombospondins attenuate EC proliferation and migration *in vitro* and inhibit angiogenesis *in vivo*, which is strictly dependent on their interaction with the CD36 receptor. CD36 has previously been shown to be regulated by different PPAR subtypes in a variety of cell types (Tontonoz *et al*, 1998; Westergaard *et al*, 2001; Sato *et al*, 2002; Liu *et al*, 2004), consistent with the present observations. In *Pparb*$^{-/-}$ cells, both ligand *(Thbs2)* and receptor *(Cd36)* genes are downregulated, suggesting that a signaling loop with an essential function in modulating angiogenesis might be impaired in these cells. CD36 and thrombospondin would have a similar effect on EC proliferation as p57^{KIP2}, suggesting that these molecules may act in concert. We have also identified a number of other genes with potential functions in growth control and differentiation that show a decreased expression in matrigel-invading cells from *Pparb*$^{-/-}$ mice (see highlighted entries in Supplementary Table S1; Figure 8). Interestingly, further backcrossing of the *Pparb*$^{-/-}$ strain to C57BL/6N mice results in a lower incidence of tumor resistance (our unpublished observation), suggesting that strain-specific modifier loci also influence the observed phenotype. At present, it is therefore not possible to distinguish which of these genes play a role in the context of PPARβ-dependent vascularization, but it is very likely that multiple target genes are involved.

Conclusions

The angiogenic response to growth factors during the final stages of tumor angiogenesis is characterized by an inhibition of EC proliferation and the acquisition of a fully differentiated phenotype (Carmeliet, 2000). Our findings are consistent with a model where PPARβ is required at this stage of tumor angiogenesis, where it functions to attenuate EC proliferation as a prerequisite for microvessel maturation/differentiation. Thus, the loss of PPARβ does not interfere with angiogenesis *per se*, but rather results in the deregulation of angiogenesis, leading to a hyperplastic phenotype and the formation of non-functional microvessels. It is likely that the reduced PPARβ-dependent expression of *Cdkn1c* is at least in part responsible for the phenotype seen in $Pparb^{-/-}$ mice, as suggested by its role in the PPARβ-mediated inhibition of cultured cells. Thus, *Cdkn1c* has the potential to impinge on tumor growth in different ways. When expressed in the tumor cells proper, *Cdkn1c* inhibits tumorigenesis by a direct inhibitory effect of tumor cell proliferation (Kuang *et al*, 2007), while its expression in tumor EC cells is required for blood vessel formation and thus tumor growth.

A similar phenotype of enhanced, but non-productive angiogenesis has very recently been described in mice lacking the Notch ligand Delta-Like 4 (Dll4), or mice systemically treated with a Dll4-neutralizing antibody (Noguera-Troise *et al*, 2006; Ridgway *et al*, 2006). The lack of functional Dll4 rendered angiogenic ECs hyperproliferative and markedly increased tumor vascularity, but caused defective microvessel differentiation and blocked syngeneic tumor growth. Even though the histological evidence (hyperplasia and immature microvessels lacking a lumen) and the functional consequences on tumor growth are strikingly similar to our observations with $Pparb^{-/-}$ mice, there are clear differences and probably no functional links. Most importantly, Dll4 is essential for embryonic vascular development and arteriogenesis (Krebs *et al*, 2004), whereas PPARb is not required for physiological angiogenesis. Furthermore, we were unable to detect any differences in the expression of *Dll4* or other key component of Notch signaling between $Pparb^{+/+}$ and $Pparb^{-/-}$ cells from matrigel plugs (data not shown). This suggests that multiple and presumably independent mechanism are required to prevent the deregulation of tumor EC proliferation and the occurrence of non-productive angiogenesis. It is possible that due to the highly pathological tumor micro-environment, tumor-specific regulatory mechanisms have to be operational to prevent an excessive angiogenic response of the tumor stroma. Our results suggest that Pparβ is such a regulator. Our findings that *Pparb* is the predominantly expressed *Ppar* subtype in angiogenic matrigel plugs and human tumor ECs, and is inducible by angiogenic growth factors *in vitro*, supports this hypothesis.

Previous studies addressing the role of PPARβ in tumorigenesis have yielded partly conflicting results (Park *et al*, 2001; Barak *et al*, 2002; Gupta *et al*, 2004; Harman *et al*, 2004; Reed *et al*, 2004; Marin *et al*, 2006), leaving it unclear whether PPARβ has tumor promoting or suppressing properties. Our findings possibly help to shed light on this issue. PPARβ may have different functions in tumor stroma and in certain tumor cells with opposing effects on tumor growth. Clearly, a detailed understanding of these complexities will be a prerequisite for the development of PPARβ-directed drugs and their clinical application.

Materials and methods

Cell culture

Lewis lung carcinoma (LLC1) and B16F1 melanoma were obtained from the ATCC and cultured in DMEM plus 10% fetal bovine serum. Aortic ECs were isolated as described (Chen *et al*, 2004). HuVECs were established and cultured as described (Graulich *et al*, 1999). Cell lines obtained from $Pparb^{+/+}$, $Pparb^{-/-}$ and *Flox-Pparb* ($PPAR\delta^{ck}$) mice are described in Supplementary data. Retroviral infections, siRNA transfections and luciferase assays are described in Supplementary data.

Mouse strains

$Pparb^{-/-}$ and $Pparb^{+/+}$ mice have previously been described (Peters *et al*, 2000). All experiments were performed with mice backcrossed with the C57BL/6N strain. $PPAR\delta^{ck}$ mice (Barak *et al*, 2002) harboring a floxed *Pparb* exon 4 were kindly provided by R Evans (The Salk Institute, La Jolla, CA).

Matrigel plug assay

Matrigel plugs (Ley *et al*, 2004) were established using the BD Matrigel Matrix (Becton Dickinson), as described by the manufacturer. In brief, 500 μl of liquefied matrigel containing 100 nM PGE_2 and 0.6 μg/ml FGF-2 were injected subcutaneously and plugs were removed 3 days later for analysis. For retroviral 'rescue' experiments, 10^5 stably transduced fibroblasts (see below) were harvested during the exponential growth phase and included in the matrigel.

MRI

Dynamic gadolinium Gd-DTPA enhanced imaging (Choyke *et al*, 2003; Kiessling *et al*, 2003) was carried out with a clinical 1.5 T whole-body MRI-System (Siemens Sonata, Erlangen, Germany) and a dedicated custom-made small animal coil. Mice were anesthetized, injected i.v. with 0.5 mmol/kg of Gd-DTPA, and imaging was started immediately thereafter. We performed 510 measurements per session during a total period of 9 min.

Immunohistology

Paraffin-embedded sections were stained as described in Supplementary data. The following antibodies were used: α-SMA (peroxidase-conjugated, Sigma, Munich, Germany), FLAG tag (Becton Dickinson, Heidelberg, Germany), PCNA (polyclonal FL-261, Santa Cruz Biotechnology, Santa Cruz, California, USA) and AQP-1 (kind gift from Dr S Nielsen, Aarhus, Denmark) (Gresz *et al*, 2001). Signals were visualized by biotinylated secondary antibodies and either avidin-conjugated peroxidase with diaminobenzidine as the substrate, or avidin-conjugated alkaline phosphatase with Vector® Red (Vector Lab, California, USA). Double immunofluorescence was performed using an FITC-labeled α-SMA antibody and the polyclonal rabbit anti-AQP-1 antibody with a Cy5-labeled secondary antibody.

Microarrays

Microarrays were generated using a GMS 417 arrayer (MWG Biotech, Ebersberg, Germany). The chips contained 22 500 clones from the mouse sequence-verified NIA 15k cDNA library plus the NIA 7.4k cDNA clone set (http://lgsun.grc.nia.nih.gov/cDNA/cDNA.html). Analyses were performed with amplified RNA (Supplementary data). Each experiment was performed as a sandwich hybridization using two arrays, and two independent experiments were performed for each data point. Spot intensities were analyzed from scanned images using Scan Array Express™ (Perkin Elmer, Rodgau, Germany). Data from all four hybridization were averaged before further analysis. All procedures were performed according to the protocols described at http://www.imt.uni-marburg.de/microarray/download.html.

Supplementary data

Supplementary data are available at *The EMBO Journal* Online (http://www.embojournal.org).

Acknowledgements

We thank Dr R Evans (Salk Institute, La Jolla, CA) for PPARδ^{ck} mice, Dr T Blankenstein (MDC Berlin, Germany) for the retroviral Cre vector, Dr S Nielsen (Aarhus, Denmark) for providing the polyclonal AQP-1 antibody. We are grateful to Birgit Samans, Dr M Krause and Professor M Eilers for help with microarray analyses, to Lena Holembowski for *Cdkn1c* promoter experiments, and to Bernhard Wilke, Julia Dick, Margitta Alt, Christine Rösser and Renate Baumann for excellent technical assistance. This work was supported by grants from the Deutsche Forschungsgemeinschaft (SFB-TR17/A3), the Deutsche Krebshilfe, the Wilhelm-Sander-Stiftung and the National Cancer Institute (CA89607, CA97999, CA124533).

References

Armstrong LC, Bornstein P (2003) Thrombospondins 1 and 2 function as inhibitors of angiogenesis. *Matrix Biol* **22:** 63–71

Barak Y, Liao D, He W, Ong ES, Nelson MC, Olefsky JM, Boland R, Evans RM (2002) Effects of peroxisome proliferator-activated receptor delta on placentation, adiposity, and colorectal cancer. *Proc Natl Acad Sci USA* **99:** 303–308

Barish GD, Narkar VA, Evans RM (2006) PPAR delta: a dagger in the heart of the metabolic syndrome. *J Clin Invest* **116:** 590–597

Bissell MJ, Radisky D (2001) Putting tumours in context. *Nat Rev Cancer* **1:** 46–54

Burdick AD, Bility MT, Girroir EE, Billin AN, Willson TM, Gonzalez FJ, Peters JM (2007) Ligand activation of peroxisome proliferator-activated receptor-beta/delta(PPARbeta/delta) inhibits cell growth of human N/TERT-1 keratinocytes. *Cell Signal* **19:** 1163–1171

Burdick AD, Kim DJ, Peraza MA, Gonzalez FJ, Peters JM (2006) The role of peroxisome proliferator-activated receptor-beta/delta in epithelial cell growth and differentiation. *Cell Signal* **18:** 9–20

Carmeliet P (2000) Mechanisms of angiogenesis and arteriogenesis. *Nat Med* **6:** 389–395

Chen S, Sega M, Agarwal A (2004) 'Lumen digestion' technique for isolation of aortic endothelial cells from heme oxygenase-1 knockout mice. *Biotechniques* **37:** 84–89

Choyke PL, Dwyer AJ, Knopp MV (2003) Functional tumor imaging with dynamic contrast-enhanced magnetic resonance imaging. *J Magn Reson Imaging* **17:** 509–520

Desvergne B, Michalik L, Wahli W (2006) Transcriptional regulation of metabolism. *Physiol Rev* **86:** 465–514

Feige JN, Gelman L, Michalik L, Desvergne B, Wahli W (2006) From molecular action to physiological outputs: peroxisome proliferator-activated receptors are nuclear receptors at the crossroads of key cellular functions. *Prog Lipid Res* **45:** 120–159

Folkman J (2002) Role of angiogenesis in tumor growth and metastasis. *Semin Oncol* **29:** 15–18

Forman BM, Chen J, Evans RM (1997) Hypolipidemic drugs, polyunsaturated fatty acids, and eicosanoids are ligands for peroxisome proliferator-activated receptors alpha and delta. *Proc Natl Acad Sci USA* **94:** 4312–4317

Graulich W, Nettelbeck DM, Fischer D, Kissel T, Muller R (1999) Cell type specificity of the human endoglin promoter. *Gene* **227:** 55–62

Gresz V, Kwon TH, Hurley PT, Varga G, Zelles T, Nielsen S, Case RM, Steward MC (2001) Identification and localization of aquaporin water channels in human salivary glands. *Am J Physiol Gastrointest Liver Physiol* **281:** G247–G254

Gupta RA, Wang D, Katkuri S, Wang H, Dey SK, DuBois RN (2004) Activation of nuclear hormone receptor peroxisome proliferator-activated receptor-delta accelerates intestinal adenoma growth. *Nat Med* **10:** 245–247

Harman FS, Nicol CJ, Marin HE, Ward JM, Gonzalez FJ, Peters JM (2004) Peroxisome proliferator-activated receptor-delta attenuates colon carcinogenesis. *Nat Med* **10:** 481–483

Kawamoto A, Tkebuchava T, Yamaguchi J, Nishimura H, Yoon YS, Milliken C, Uchida S, Masuo O, Iwaguro H, Ma H, Hanley A, Silver M, Kearney M, Losordo DW, Isner JM, Asahara T (2003) Intramyocardial transplantation of autologous endothelial progenitor cells for therapeutic neovascularization of myocardial ischemia. *Circulation* **107:** 461–468

Kiessling F, Krix M, Heilmann M, Vosseler S, Lichy M, Fink C, Farhan N, Kleinschmidt K, Schad L, Fusenig NE, Delorme S (2003) Comparing dynamic parameters of tumor vascularization in nude mice revealed by magnetic resonance imaging and contrast-enhanced intermittent power Doppler sonography. *Invest Radiol* **38:** 516–524

Kim DJ, Bility MT, Billin AN, Willson TM, Gonzalez FJ, Peters JM (2006) PPARbeta/delta selectively induces differentiation and inhibits cell proliferation. *Cell Death Differ* **13:** 53–60

Kim DJ, Murray IA, Burns AM, Gonzalez FJ, Perdew GH, Peters JM (2005) Peroxisome proliferator-activated receptor-beta/delta inhibits epidermal cell proliferation by downregulation of kinase activity. *J Biol Chem* **280:** 9519–9527

Kitz Kramer D, Al-Khalili L, Guigas B, Leng Y, Garcia-Roves PM, Krook A (2007) Role of AMP kinase and PPARdelta in the regulation of lipid and glucose metabolism in human skeletal muscle. *J Biol Chem* **280:** 19313–19320

Krebs LT, Shutter JR, Tanigaki K, Honjo T, Stark KL, Gridley T (2004) Haploinsufficient lethality and formation of arteriovenous malformations in Notch pathway mutants. *Genes Dev* **18:** 2469–2473

Kuang SQ, Ling X, Sanchez-Gonzalez B, Yang H, Andreeff M, Garcia-Manero G (2007) Differential tumor suppressor properties and transforming growth factor-beta responsiveness of p57KIP2 in leukemia cells with aberrant p57KIP2 promoter DNA methylation. *Oncogene* **26:** 1439–1448

Lee CH, Chawla A, Urbiztondo N, Liao D, Boisvert WA, Evans RM, Curtiss LK (2003) Transcriptional repression of atherogenic inflammation: modulation by PPARdelta. *Science* **302:** 453–457

Lee MH, Reynisdottir I, Massague J (1995) Cloning of p57KIP2, a cyclin-dependent kinase inhibitor with unique domain structure and tissue distribution. *Genes Dev* **9:** 639–649

Ley CD, Olsen MW, Lund EL, Kristjansen PE (2004) Angiogenic synergy of bFGF and VEGF is antagonized by Angiopoietin-2 in a modified *in vivo* Matrigel assay. *Microvasc Res* **68:** 161–168

Li LP, Schlag PM, Blankenstein T (1997) Transient expression of SV 40 large T antigen by Cre/LoxP-mediated site-specific deletion in primary human tumor cells. *Hum Gene Ther* **8:** 1695–1700

Liu Y, Zhu Y, Rannou F, Lee TS, Formentin K, Zeng L, Yuan X, Wang N, Chien S, Forman BM, Shyy JY (2004) Laminar flow activates peroxisome proliferator-activated receptor-gamma in vascular endothelial cells. *Circulation* **110:** 1128–1133

Marin HE, Peraza MA, Billin AN, Willson TM, Ward JM, Kennett MJ, Gonzalez FJ, Peters JM (2006) Ligand activation of peroxisome proliferator-activated receptor beta inhibits colon carcinogenesis. *Cancer Res* **66:** 4394–4401

Michalik L, Desvergne B, Tan NS, Basu-Modak S, Escher P, Rieusset J, Peters JM, Kaya G, Gonzalez FJ, Zakany J, Metzger D, Chambon P, Duboule D, Wahli W (2001) Impaired skin wound healing in peroxisome proliferator-activated receptor (PPAR)alpha and PPARbeta mutant mice. *J Cell Biol* **154:** 799–814

Nadra K, Anghel SI, Joye E, Tan NS, Basu-Modak S, Trono D, Wahli W, Desvergne B (2006) Differentiation of trophoblast giant cells and their metabolic functions are dependent on peroxisome proliferator-activated receptor beta/delta. *Mol Cell Biol* **26:** 3266–3281

Noguera-Troise I, Daly C, Papadopoulos NJ, Coetzee S, Boland P, Gale NW, Lin HC, Yancopoulos GD, Thurston G (2006) Blockade of Dll4 inhibits tumour growth by promoting non-productive angiogenesis. *Nature* **444:** 1032–1037

Park BH, Vogelstein B, Kinzler KW (2001) Genetic disruption of PPARdelta decreases the tumorigenicity of human colon cancer cells. *Proc Natl Acad Sci USA* **98:** 2598–2603

Peraza MA, Burdick AD, Marin HE, Gonzalez FJ, Peters JM (2006) The toxicology of ligands for peroxisome proliferator-activated receptors (PPAR). *Toxicol Sci* **90:** 269–295

Peters JM, Lee SS, Li W, Ward JM, Gavrilova O, Everett C, Reitman ML, Hudson LD, Gonzalez FJ (2000) Growth, adipose, brain, and skin alterations resulting from targeted disruption of the mouse peroxisome proliferator-activated receptor beta(delta). *Mol Cell Biol* **20:** 5119–5128

Reed KR, Sansom OJ, Hayes AJ, Gescher AJ, Winton DJ, Peters JM, Clarke AR (2004) PPARdelta status and Apc-mediated tumourigenesis in the mouse intestine. *Oncogene* **23:** 8992–8996

Ridgway J, Zhang G, Wu Y, Stawicki S, Liang WC, Chanthery Y, Kowalski J, Watts RJ, Callahan C, Kasman I, Singh M, Chien M, Tan C, Hongo JA, de Sauvage F, Plowman G, Yan M (2006) Inhibition of Dll4 signalling inhibits tumour growth by deregulating angiogenesis. *Nature* **444:** 1083–1087

Saadoun S, Papadopoulos MC, Hara-Chikuma M, Verkman AS (2005) Impairment of angiogenesis and cell migration by targeted aquaporin-1 gene disruption. *Nature* **434:** 786–792

Samuelsson MK, Pazirandeh A, Davani B, Okret S (1999) p57Kip2, a glucocorticoid-induced inhibitor of cell cycle progression in HeLa cells. *Mol Endocrinol* **13:** 1811–1822

Sato O, Kuriki C, Fukui Y, Motojima K (2002) Dual promoter structure of mouse and human fatty acid translocase/CD36 genes and unique transcriptional activation by peroxisome proliferator-activated receptor alpha and gamma ligands. *J Biol Chem* **277:** 15703–15711

Schmuth M, Haqq CM, Cairns WJ, Holder JC, Dorsam S, Chang S, Lau P, Fowler AJ, Chuang G, Moser AH, Brown BE, Mao-Qiang M, Uchida Y, Schoonjans K, Auwerx J, Chambon P, Willson TM, Elias PM, Feingold KR (2004) Peroxisome proliferator-activated receptor (PPAR)-beta/delta stimulates differentiation and lipid accumulation in keratinocytes. *J Invest Dermatol* **122:** 971–983

Tan NS, Michalik L, Noy N, Yasmin R, Pacot C, Heim M, Fluhmann B, Desvergne B, Wahli W (2001) Critical roles of PPAR beta/delta in keratinocyte response to inflammation. *Genes Dev* **15:** 3263–3277

Tontonoz P, Nagy L, Alvarez JG, Thomazy VA, Evans RM (1998) PPARgamma promotes monocyte/macrophage differentiation and uptake of oxidized LDL. *Cell* **93:** 241–252

Varnat F, Heggeler BB, Grisel P, Boucard N, Corthesy-Theulaz I, Wahli W, Desvergne B (2006) PPARbeta/delta regulates paneth cell differentiation via controlling the hedgehog signaling pathway. *Gastroenterology* **131:** 538–553

Westergaard M, Henningsen J, Svendsen ML, Johansen C, Jensen UB, Schroder HD, Kratchmarova I, Berge RK, Iversen L, Bolund L, Kragballe K, Kristiansen K (2001) Modulation of keratinocyte gene expression and differentiation by PPAR-selective ligands and tetradecylthioacetic acid. *J Invest Dermatol* **116:** 702–712

Zhang P, Liegeois NJ, Wong C, Finegold M, Hou H, Thompson JC, Silverman A, Harper JW, DePinho RA, Elledge SJ (1997) Altered cell differentiation and proliferation in mice lacking p57KIP2 indicates a role in Beckwith–Wiedemann syndrome. *Nature* **387:** 151–158

